Published in final edited form as:
Sci Transl Med. 2012 October 10; 4(155): 155ra137. doi:10.1126/scitranslmed.3004373.

Neural Stem Cell Engraftment and Myelination in the Human Brain

Nalin Gupta[1,2], **Roland G. Henry**[3,4,5], **Jonathan Strober**[2,3], **Sang-Mo Kang**[6], **Daniel A. Lim**[1], **Monica Bucci**[3], **Eduardo Caverzasi**[3], **Laura Gaetano**[3], **Maria Luisa Mandelli**[3], **Tamara Ryan**[7], **Rachel Perry**[7], **Jody Farrell**[7], **Rita J. Jeremy**[8], **Mary Ulman**[2], **Stephen L. Huhn**[9], **A. James Barkovich**[2,3,4], and **David H. Rowitch**[1,2,10,*]

[1]Department of Neurological Surgery, University of California, San Francisco, San Francisco, CA 94143, USA

[2]Department of Pediatrics, University of California, San Francisco, San Francisco, CA 94143, USA

[3]Department of Neurology, University of California, San Francisco, San Francisco, CA 94143, USA

[4]Department of Radiology, University of California, San Francisco, San Francisco, CA 94143, USA

[5]Bioengineering Graduate Group, University of California, San Francisco, San Francisco, CA 94143, USA

[6]Division of Transplantation, Department of Surgery, University of California, San Francisco, San Francisco, CA 94143, USA

[7]Fetal Treatment Center, University of California, San Francisco, San Francisco, CA 94143, USA

[8]Clinical & Translational Science Institute, University of California, San Francisco, San Francisco, CA 94143, USA

[9]StemCells Inc., Newark, CA 94560, USA

[10]Howard Hughes Medical Institute

Abstract

[*]To whom correspondence should be addressed. rowitchd@peds.ucsf.edu.

Author contributions: N.G. performed the surgical procedures and contributed to the writing of the paper; R.G.H. analyzed the MRI data and contributed to the writing of the paper; J.S. compiled and analyzed the clinical data and contributed to the writing of the paper; S.-M.K. analyzed the immunosuppression results; D.A.L. assisted with the surgical procedures; M.B., E.C., L.G., and M.L.M. analyzed the MRI data; T.R., R.P., and J.F. conducted the clinical evaluations and compiled the clinical data; R.J.J. performed and analyzed the neuropsychological data; M.U. contributed to the study design and the writing of the paper; S.L.H. contributed to the study design, analysis of data, and writing of the paper; A.J.B. analyzed the MRI data and contributed to the writing of the paper; and D.H.R. was responsible for the overall conduct of the study, data analysis, and writing of the paper.

SUPPLEMENTARY MATERIALS

www.sciencetranslationalmedicine.org/cgi/content/full/4/155/155ra137/DC1

Competing interests: D.H.R. has nothing to disclose. S.L.H. is employed by the sponsor StemCells Inc., and other primary study personnel (N.G., R.G.H., J.S., S.-M.K., T.R., R.P., R.J.J., M.U., and A.J.B.) received partial salary support from the sponsor. HuCNS-SC for use in PMD is claimed by a host of U.S. patents issued to StemCells Inc.: U.S. patent nos. 5,968,829 (“Human CNS neural stem cells”); 7,361,505 (“Multipotent neural stem cell compositions”); 7,153,686 (“Compositions of enriched central nervous system stem cell and progenitor cell populations”); 6,777,233 (“Cultures of human CNS neural stem cells”); 5,851,832 (“In vitro growth and proliferation of multipotent neural stem cells and their progeny”); 6,497,872 (“Neural transplantation using proliferated multipotent neural stem cells and their progeny”); and 7,166,277 (“Remyelination of neurons using multipotent neural stem cell progeny”).

Pelizaeus-Merzbacher disease (PMD) is a rare leukodystrophy caused by mutation of the *proteolipid protein 1* gene. Defective oligodendrocytes in PMD fail to myelinate axons, causing global neurological dysfunction. Human central nervous system stem cells (HuCNS-SCs) can develop into oligodendrocytes and confer structurally normal myelin when transplanted into a hypomyelinating mouse model. A 1-year open-label phase 1 study was undertaken to evaluate safety and to detect evidence of myelin formation after HuCNS-SC transplantation. Allogeneic HuCNS-SCs were surgically implanted into the frontal lobe white matter in four male subjects with an early-onset severe form of PMD. Immunosuppression was administered for 9 months. Serial neurological evaluations, developmental assessments, and cranial magnetic resonance imaging (MRI) and MR spectroscopy, including high-angular resolution diffusion tensor imaging (DTI), were performed at baseline and after transplantation. The neurosurgical procedure, immunosuppression regimen, and HuCNS-SC transplantation were well tolerated. Modest gains in neurological function were observed in three of the four subjects. No clinical or radiological adverse effects were directly attributed to the donor cells. Reduced T1 and T2 relaxation times were observed in the regions of transplantation 9 months after the procedure in the three subjects. Normalized DTI showed increasing fractional anisotropy and reduced radial diffusivity, consistent with myelination, in the region of transplantation compared to control white matter regions remote to the transplant sites. These phase 1 findings indicate a favorable safety profile for HuCNS-SCs in subjects with PMD. The MRI results suggest durable cell engraftment and donor-derived myelin in the transplanted host white matter.

INTRODUCTION

Oligodendrocytes of the central nervous system (CNS) function primarily to myelinate axons and enhance nerve conduction. Pelizaeus-Merzbacher disease (PMD) is a rare congenital X-linked recessive leukodystrophy caused by mutation of myelin protein *proteolipid protein 1* (*PLP1*) (1), resulting in hypomyelination with an innate but not an autoimmune inflammatory component (2). One of a recognized group of “hypomyelinating disorders” (2), PMD has an incidence of 1:200,000 to 1:500,000; the subset of these patients affected with the early-onset severe (that is, connatal) form of PMD present with profound neurodevelopmental deficits. In patients with PMD, oligodendrocytes are unable to myelinate axons, resulting in loss of normal axonal conduction and neurological dysfunction in the short term, eventually leading to axonopathy and neurodegeneration.

Both gene duplications and point mutations of *PLP1* can result in marked hypomyelination of the CNS (3). Various *PLP1* mutations result in abnormal myelin production (4) or abnormal trafficking in the endoplasmic reticulum of oligodendrocytes, leading to apoptosis by activation of the unfolded protein response (5, 6). Because *PLP1* is only expressed in oligodendrocytes of the CNS, the pathobiology of PMD is cell type–restricted. Therefore, oligodendrocyte cellular replacement has been proposed as a therapeutic approach (7).

Animal models relevant to PMD show a spectrum of hypomyelination, seizures, and early postnatal lethality (4). These models have also provided further insight into possible disease mechanisms and a useful platform for testing therapeutic approaches (5, 6, 8). Transplantation of human glial progenitor cells into the brains of hypomyelinated *shiverer* (*Shi*) mice results in functional engraftment and donor-derived myelination that is progressive with time (9). This is in keeping with known biological properties of oligodendrocyte precursors that migrate and proliferate after specification (10). Human CNS stem cells (HuCNS-SCs), also referred to as neural stem cells, show the properties of self-renewal and multipotency in vitro and have been shown to produce oligodendrocytes that generate compact myelin and to normalize nodal organization and functional axonal conduction velocities in the *Shi* mouse model (11, 12).

Magnetic resonance (MR) diffusion tensor imaging (DTI) quantifies differences in the magnitude and direction of water motion that result from myelination and is routinely used in diagnosis and clinical characterization of demyelinating diseases in humans such as multiple sclerosis. This MR technique has also been studied in experimental models of hypomyelination (12, 13) and remyelination (14, 15). The MR results obtained in these relevant animal models suggest that MR imaging (MRI)–DTI is an excellent tool to noninvasively assess changes after transplantation. We performed a study in subjects with early-severe PMD to evaluate safety and clinical effects of HuCNS-SC transplantation in the setting of a progressive neurodegenerative disorder with diffuse hypomyelination. We used MR-DTI as a sensitive measure of myelination after HuCNS-SC transplantation.

RESULTS

Study design and patient selection

This study was conducted as an open-label phase 1 trial in four subjects with the early-severe form of PMD (ClinicalTrials.gov NCT01005004). The U.S. Food and Drug Administration (FDA)–authorized study protocol had oversight from the Committee for Human Research and Gamete, Embryo, and Stem Cell Research Committees at the University of California, San Francisco (UCSF). PMD is a fatal disease with no approved treatments, and the UCSF oversight committees found that the trial qualified for offering the prospect of direct clinical benefit according to the guidelines in the Code of Federal Regulations (21CFR50.52).

Prescreening of 17 potential subjects identified 6 that met eligibility criteria (table S1) and were formally evaluated at the study center. Of these six possible subjects, one family declined participation, whereas another potential subject became Epstein-Barr virus (EBV)–positive before enrollment, resulting in exclusion. All families of study subjects provided written informed consent. The study protocol included a single-stage transplant procedure followed by immunosuppression for a period of 9 months. A minimum of 28 days was required between dosing of consecutive subjects, and an independent Data Monitoring Committee reviewed the accruing safety data before each transplant. Subjects returned to UCSF for frequent clinical and imaging assessment for a year after transplant (table S2). The phase 1 study was carried out between January 2010 and February 2012. Subjects were enrolled in a separate 4-year long-term follow-up study after the final 12-month assessment of the phase 1 study.

Eligible subjects were males 6 months to 5 years of age with mutations in *PLP1*, absence of myelination by MRI, and clinical manifestations of early-severe PMD. Early-severe PMD was characterized by the onset of documented nystagmus by 3 months of age, severe developmental delay, and failure to attain normal gross motor milestones within 6 months of age (Table 1). Subjects 1, 3, and 4 had histories of neonatal stridor (breathing difficulty), and two (subjects 1 and 3) required tracheostomy and gastrostomy tube placement shortly after birth. All subjects underwent a total of at least eight detailed posttransplant neurological examinations that were also videotaped for post hoc review. Mental status examination revealed that all subjects were awake and alert but with little facial animation evident and some baseline irritability. Subjects 1 and 3 were 16 and 14 months of age at the time of study entry, respectively, and were noted to have minimal or no antigravity motor movement (Table 1). Subjects 2 and 4 were 3 and 5 years of age at the time of study entry, respectively, and showed antigravity strength throughout, marked dysmetria, and minimal truncal support. Subject 4 also had the capability of very limited walker use with significant support. Subjects 2 and 4 were generally interactive with the ability to create some sounds or single words, as well as follow one-step commands at study entry.

The neuropsychological and developmental assessments included the Bayley Scales of Infant and Toddler Development, Third Edition (Bayley-III), the Callier-Azusa Scale G (CAS), and the Functional Independence Measure for Children (WeeFIM). Quality of life was assessed with the Child Health Questionnaire Parent Form (CHQ-PF50). All subjects also underwent routine electroencephalogram (EEG), somatosensory evoked potentials (SSEPs), and neuro-ophthalmological evaluations (table S2).

Transplantation of HuCNS-SCs into patients with PMD

The isolation and purification of HuCNS-SCs have been previously described (16) (see Materials and Methods). HuCNS-SCs are multipotent neural stem cells (CD133-, nestin-, and Sox2-positive) that are expanded in culture as neurospheres (16, 17), and then cryopreserved into master and working cell banks, from which patient lots are derived for transplantation. The biological multipotent properties of the purified and expanded human neural stem cells have been well characterized (11, 18), and their ability to produce functional myelin is described in a companion paper (12).

HuCNS-SC (16) banks and patient lots were produced under current Good Manufacturing Practice (GMP). Furthermore, to conform to the FDA's requirements for cell-based products, karyotype analysis and extensive release testing for infectious agents were performed on the cell banks used in this clinical study. In addition to release testing, extensive preclinical Good Laboratory Practice (GLP) animal testing to assess potential for tumor formation and distribution to other organs was performed, and the results were included as part of the documentation required for regulatory authorization of the trial by the FDA. HuCNS-SCs are fetal brain–derived neural stem cells (see Materials and Methods) and are not known to carry the tumorigenic risk associated with embryonic stem (ES) or induced pluripotent stem (iPS) cells. Viability and sterility of products were performed by the study sponsor (StemCells Inc.) for each patient sample. The HuCNS-SCs intended for transplant were provided as a single-use injectable suspension, and all the doses supplied in the study originated from a single donor.

HuCNS-SC transplantation was performed through four bilateral frontal burr holes to target the anterior and posterior frontal centrum semiovale or corona radiata (Fig. 1). A dual side-port 20-gauge needle was advanced to a depth of at least 2 cm below the cortical surface at each target site of the precentral centrum semiovale white matter using MRI-based stereotactic navigation. A total brain dose of 3.0×10^8 HuCNS-SCs was administered to each subject. The total dose was divided into four equal aliquots of 7.5×10^7 cells in 1 ml of cell suspension into each of the four frontal lobe sites. The dose was calculated for safety purposes on the basis of previous human safety experience (ClinicalTrials.gov NCT00337636) of HuCNS-SC injection into subjects with neuronal ceroid lipofuscinosis in which a 1-ml suspension containing 50 to 100 million cells was well tolerated.

The immunosuppression regimen consisted of oral tacrolimus with a target level of 5 to 10 ng/ml for the first 28 days after transplant and then a lower target level of 2 to 5 ng/ml until discontinuation at the end of 9 months after transplant. Mycophenolate mofetil was also administered for the first 28 days after transplant. Prophylaxis with sulfamethoxazole and trimethoprim (SMZ-TMP) was continued from day 3 to 9 months after transplant. A solid-organ transplant physician supervised administration of immunosuppressive agents. Safety parameters included general physical, neurologic, neurophysiologic, neurodevelopmental, and ophthalmologic assessment (see below); blood and urine analysis; electrocardiogram; chest x-ray; and MRI at routine intervals (table S2).

Safety and clinical outcomes

A total of 54 nonserious adverse events and 2 serious adverse events were collected during the study. The most common nonserious adverse events reported more than once included, in order of decreasing frequency, rashes ($n = 5$), diarrhea ($n = 4$), fever ($n = 3$), rhinorrhea ($n = 2$), and decreased serum bicarbonate ($n = 2$). Subject 1 developed a subgaleal pseudomeningocele (fluid collection under the scalp) after surgery that resolved spontaneously. Small cortical/subcortical hemorrhages were observed on the immediate postoperative head computed tomography (CT) beneath the postsurgical cranial defects in subject 2; these had no mass effect and were without clinical consequence. Two serious adverse events occurred in the same subject (both were hospital admissions for exacerbation of baseline tracheitis and/or a viral syndrome); neither was considered related to the HuCNS-SC transplant. Immunosuppression was generally well tolerated, with no evidence of opportunistic infections. Subject 2 converted to EBV immunoglobulin G (IgG)–positive only (IgM-negative) at 12 months after transplant without a clinical correlate. Subject 3 was switched from SMZ-TMP to atovaquone because of a rash on day 14. We did not identify by serial MRI any signs of abnormal gadolinium enhancement, neoplasia, ischemia, or inflammation in any subject.

The neurologic examination 12 months after transplantation in all subjects revealed either stable or modest gains in motor and mental status function compared to the pretransplant examination. Subject 1 showed no signs of neurological improvement, but his requirement for nightly continuous positive airway pressure (CPAP) was reduced over the course of 12 months after transplant. Subject 2 developed improved truncal support and the ability to take steps with assistance and began speaking audible single words with the ability to follow two-step commands. Subject 3 developed antigravity strength in his upper extremities, started taking solid foods orally, and had reduced nightly CPAP requirements. Subject 4 developed improved truncal support and progressed from requiring significant support with use of the walker at baseline to walking with minimal assistance at the 12-month examination. Subject 4 also developed the ability to follow two-steps commands and self-feed. Although the above neurological gains were considered modest and variable across subjects, clinical changes were progressive from about 6 to 9 months after transplantation and persisted after cessation of immunosuppression. No subjects developed seizure activity, and SSEP and neuro-ophthalmology examination results did not change from baseline in any subject during the year after transplant.

The neuropsychological assessments with the Bayley-III, CAS (Fig. 2), and WeeFIM showed overall stability for all subjects compared to baseline. The low level of cognitive function evident in each test at baseline reflected the dense CNS disability associated with connatal PMD, and most subjects scored at the very extreme limits of the testing scale across most subsets. The severe level of impairment present in PMD subjects makes detection of small changes in cognitive function difficult. Nonetheless, small but measurable gains were observed in select subtests of the Bayley-III, CAS, and WeeFIM for subjects 2 to 4. Of the three, subject 2 had the most definitive gains characterized by changes in receptive and expressive language function on the Bayley-III from 6 and 8 months of developmental age at baseline to 13 and 14 months, respectively, at the year-end assessment. The Child Health Questionnaire Parent Form (CHQ-PF50) showed no significant changes from baseline.

Brain imaging of PMD patients receiving a HuCNS-SC transplant

MRI/MR spectroscopy (MRS)/DTI was performed before transplant (baseline) and then repeated at 3, 6, 9, 10, and 12 months after transplant. The MRI scans at baseline and at 12 months included gadopentetic acid, a vascular enhancing agent used in detection of tumors

and inflammation. Single-voxel proton spectroscopy was performed in a large region of interest (ROI) (3 cm × 2 cm × 2 cm) that included the central portion of the centrum semiovale using a PRESS (point-resolved spectroscopy) technique [repetition time (TR) = 1500 ms, echo time (TE) = 26, 288 ms, number of excitations = 2]. MR DTI is considered a sensitive method for detection of myelin development and was an important component of the imaging data collected in this study. DTI allowed quantification of the magnitude (mean diffusivity), direction (radial versus axial diffusivity), and coherence (fractional anisotropy) of random water motion in localized brain ROIs containing white matter composed of bundles of aligned axons, glial cell populations, and myelin. Increased fractional anisotropy, coupled with decreased radial diffusivity and mean diffusivity, and stable axial diffusivity indicate reduced water motion perpendicular to the axis of axons and are thought to be consistent with myelin development (19).

DTI analysis was applied to the ROIs that received HuCNS-SC transplants within the central corona radiata and was compared to DTI analysis of multiple ROIs in white matter remote to the transplant sites (genu and splenium of the corpus callosum, anterior frontal corona radiata white matter, and posterior parieto-occipital white matter) (Fig. 3).

MRI volumetric studies of the whole brain, cerebrospinal fluid (CSF), and white/gray matter compartments showed no changes from baseline for the older subjects but increases for the younger subjects (table S3). Although preoperative MRI showed global absence of myelination, starting at the 3-month time point, we noted the development of multiple small, round/ovoid regions of reduced T1 and T2 relaxation within some implantation sites in three of the four subjects. These changes were most evident in subject 2 in which distinct foci immediately anterior to the implantation site are evident in the corona radiata on the 12-month MRI study (Fig. 4). These regions did not show enhancement after gadopentetic acid administration or the MRI, MRS, or diffusion characteristics of neoplasm, inflammation, or cysts. MRS did not change after transplantation in any of the subjects. There was no evidence of increased myo-inositol to suggest an astroglial response, nor an increase in choline to suggest inflammation or neoplasm.

Analysis of the DTI revealed increased fractional anisotropy in the ROIs located at the sites of HuCNS-SC transplantation in all four subjects (Fig. 5). The most consistent DTI changes (pronounced increases in fractional anisotropy and decreases in radial diffusivity) were detected on normalized data from subjects 2 and 4. Subject 1 showed progressive gains in fractional anisotropy but had the most variability in changes in radial diffusivity, axial diffusivity, and mean diffusivity compared to the other three subjects (Fig. 5). Subject 3 had an increase in fractional anisotropy and a reduction in radial diffusivity in the areas of transplantation, but changes of a similar magnitude were seen in the control regions as well (Fig. 5). The younger subjects (1 and 3) showed the most pronounced changes in fractional anisotropy in the control regions, which were mostly stable in the older subjects (2 and 4) (Fig. 5). Given their younger ages, the changes in control regions of subjects 1 and 3 may reflect background maturational processes not present in the older subjects.

DISCUSSION

Disorders of myelination include multiple sclerosis and cerebral palsy and are major causes of neurological mortality and morbidity (20). This phase 1 study was designed to evaluate safety and preliminary efficacy of HuCNS-SC transplantation in subjects with the early-severe (that is, connatal) form of PMD. Subjects in this small study differed in age, but all had *PLP1* mutations resulting in nonconserved amino acid substitutions in transmembrane-spanning domains (fig. S1), which might cause protein misfolding and apoptosis (5, 6). No obvious adverse clinical or radiological effects were attributed to HuCNS-SCs during the

first year after transplant. Subjects underwent rigorous surveillance, and we detected no signs of CNS neoplasia, gliosis, or inflammation by gadolinium-enhanced MRI at any point during the first year after transplant. The phase 1 results indicate a favorable safety profile at 1 year after transplant and demonstrate that the surgical intervention, immunosuppression regimen, and HuCNS-SC transplantation are feasible in subjects with an underlying severe neurodegenerative disorder. All subjects will continue to be monitored for an additional 4 years in a separate long-term follow-up study. This report adds to the human experience accruing with allogeneic fetal neural stem cell transplantation into the brain and is in keeping with safety results from another completed study conducted with HuCNS-SC transplantation, which targeted a rare lysosomal storage disease, neuronal ceroid lipofuscinosis (ClinicalTrials.gov NCT00337636) (21).

At baseline, neurological and neuropsychological profiles of our subjects indicated severe and global CNS impairment. The modest gains observed in three of the four subjects (and stability in the fourth subject) when viewed in the context of a progressive neurodegenerative disorder suggest a departure from the natural history of the disease (22). Changes in cognitive function, evident in the neuropsychological assessments, might not be expected from transplantation of the corona radiata alone, but transplanting neural stem cells with migratory capabilities into both frontal lobes could, in theory, affect cognitive performance. However, a general limitation of the phase 1 study design is the lack of a control group. Therefore, clinical outcomes in an open-label trial must be interpreted with caution because it is not possible to confirm that the neurological improvement observed is due to the experimental intervention versus other confounding variables. Ultimately, a prospective controlled study will be needed to confirm whether HuCNS-SC transplantation results in a clinical benefit, and preparation for such further study is under way. The use of surrogate radiological markers for myelination (that is, the MRI techniques described herein) will likely enhance the design of future controlled trials for rare diseases such as PMD.

There is growing interest in stem cells and oligodendrocyte precursors as potential cell-based therapeutics for treating myelination conditions (7). This clinical investigation explores the potential for donor-derived myelination after allogeneic neural stem cell transplantation in a human myelination disorder. In this regard, both conventional MRI and high-angular resolution DTI were used in this trial to noninvasively detect signals that could indicate HuCNS-SC–derived myelination against the background of diffuse hypomyelination in severe-early PMD. A limitation of our study is that alternative effects secondary to HuCNS-SC engraftment and independent of myelination cannot be excluded, and that histological confirmation of myelin formation is not feasible or ethical because of the surgical risk of stereotactic biopsies within the ROIs (23).

Qualitative changes on T1- and T2-weighted conventional MRI morphologic images in regions receiving the cell transplants were identified in three subjects; such foci became more evident with time. High-angular resolution DTI data demonstrated increased fractional anisotropy throughout the areas of transplantation, and changes were greatest at the sites of the T1 and T2 shortening. Such changes also continued to evolve over time and were generally not seen in control regions several centimeters from the implantation sites.

The DTI pattern of reduced mean diffusivity and radial diffusivity, stable axial diffusivity, and increased fractional anisotropy over time indicates a dynamic cellular process that would cause a decrease in water motion perpendicular to neuronal axons, whereas motion parallel to axons remains stable. This pattern is believed to most accurately reflect the process of myelination and has been demonstrated in animal models (12–15).

Our data describe the character and magnitude of diffusion changes in humans that have received neural stem cell transplants. The observed changes appear consistent with previous findings in a hypomyelinating animal model after transplantation with glial precursor cells (13). MR diffusion metrics in hypomyelinating *Shi* mice have been compared to wild-type mice and transplanted *Shi* mice (13). These findings indicate that myelination in wild-type animals increases fractional anisotropy by up to 20% and reduces radial diffusivity and mean diffusivity by ~13 and ~10%, respectively, compared to *Shi* mice (13). After transplantation of *Shi* animals with glial precursors, the fractional anisotropy increased by 8 to 15% in different voxels (13). The magnitude of these reported myelin-associated values is consistent with what we observed in the human corona radiata (our subjects showed 4 to 12% increase in fractional anisotropy) despite the differences (animal versus human, *Shi* versus PMD, age of subjects, and corpus callosum versus corona radiata).

In the normal human brain, most developmental progression of DTI metrics in the corona radiata has been observed before 4 years of age, with the rate of change slowing markedly by the end of the second year (24, 25). Although prospective sequential MR observational studies are lacking in severe PMD cohorts, and we did not have longitudinal data from our subjects before transplantation, available information about severe PMD suggests little progression of myelination beyond the first year or so of life. In contrast, we found that fractional anisotropy was markedly increased in transplanted corona radiata compared to control regions in subjects 1, 2, and 4. Subject 3 had the highest increase in fractional anisotropy, but a similar magnitude of change in the control regions masked this elevation in the normalized data. Reasons for the variable magnitude of the response among the subjects are not clear. Our findings of considerable white matter maturation in control ROIs in the two younger subjects (1 and 3) raise the possibility of differing white matter substrate among subjects, although the reason for the increased maturation in these subjects (proliferation and migration of transplanted cells versus an unprecedented acceleration of myelination in untreated areas) cannot be determined from our data. The degree of fractional anisotropy increase and radial diffusivity decrease in some subjects was about 50% of the magnitude of changes seen during normal myelination in human children during the first year of life, a finding that is greater than expected in severe PMD over the course of only 1 year.

Although we also considered that imaging changes might relate to immunosuppressive therapy, this conclusion is not supported by our findings of increased and sustained DTI signals after cessation of immunosuppression as well as localization of findings to the corona radiata. Previous work indicates that rapamycin can inhibit oligodendrocyte precursor differentiation (26, 27), and thus, it is possible that immunosuppressive agents might regulate the myelination capabilities of transplanted cells. Indeed, Smith and Franklin (28) found detrimental effects of cyclophosphamide—but not cyclosporine A—during donor-derived remyelination. Brüstle *et al*. (29) transplanted mouse ES cell–derived glial precursors into the myelin-deficient rat model of PMD with cyclosporin A immunosuppression and observed donor-derived myelination. Because the mode of tacrolimus (FK506) action is similar to cyclosporin A, it is expected to be similarly permissive for myelination. Understanding the precise effects of immunosuppression in the setting of allogeneic neural stem cell transplantation and donorderived myelination will continue to evolve as this field expands.

Some other cellular explanations for the pattern of DTI changes seen in this trial, such as inflammatory, gliotic, or abnormal proliferative processes, can be excluded because of the results of the MRS exams (which would be expected to show high choline levels, but this was not observed), gadolinium-enhanced MRI (expected to show enhancement), and the principle that axial diffusivity, seen to be stable in the corona radiata of these subjects, is

typically expected to decrease in inflammatory processes because of the cellular infiltrate. Likewise, the observed DTI results in principle could be secondary to any process that results in stabilization of axonal membranes, a property that has been associated with premyelinating oligodendrocyte precursors cells (30). In hypomyelinating *jimpy* mice, endogenous astrocytes ensheath axons, which can be associated with small increases in fractional anisotropy (31). However, it is unlikely that donor-derived astrocytosis accounts for the magnitude and coherence of DTI signals we observed. Moreover, in a companion paper (12), HuCNS-SCs implanted into axon tracts of hypomyelinated *Shi* mice differentiated principally into oligodendrocytes but not astrocytes as shown by immunohistochemical analyses. Other possibilities, such as the bystander effect of neural stem cells (32) and the contribution of Schwann cells (33), are unlikely to account for our findings. Schwann cells might be produced in small numbers in the first few weeks after injury, but this is inconsistent with themagnitude and timing of our MRI-DTI results.

In conclusion, our clinical trial explored the potential for white matter restoration with neural stem cell transplantation and used MR techniques to demonstrate evidence of biological effect from allogeneic donor neural stem cells. The clinical outcomes indicate that the intervention is safe and tolerated by subjects with PMD. The biological properties of the HuCNS-SCs and the radiological findings in this study, when considered collectively, suggest donor-derived myelination in the region of cell transplantation and suggest the potential for application of this approach to other disorders of myelination.

MATERIALS AND METHODS

Human CNS stem cells

The isolation and purification of HuCNS-SCs have been previously described (16). Briefly, HuCNS-SCs were derived from a single donated fetal brain obtained through a nonprofit tissue procurement agency regulated by the FDA. The tissue was enzymatically digested to generate a single-cell suspension, and fluorescence-activated cell sorting was used to purify a population of CD133-positive and CD24-negative/low cells. This purified cell population (HuCNS-SCs) was then expanded as a neurosphere culture in serum-free, chemically defined growth medium supplemented with fibroblast growth factor 2, epidermal growth factor, and leukemia inhibitory factor by a process compliant with GMP. HuCNS-SCs, purified from a single tissue source, were cryopreserved into master and working cell banks, from which patient lots were derived for allogeneic transplantation (16, 17). These cells are considered tissue-derived somatic stem cells, express nestin and Sox2, and have been extensively characterized (11, 18). Their ability to produce functional myelin in rodents is described in detail in a companion paper (12).

Transplantation procedure

The administration of the HuCNS-SCs involved insertion of a dual side-port 20-gauge needle to a depth of at least 2 cm below the cortical surface at each target site of the precentral centrum semiovale white matter of the frontal lobe using MRI-based guidance. The injection was conducted over 10 min at each transplant site; the cortical surface overlying the needle insertion was monitored for signs of reflux, and the rate of injection was adjusted accordingly. Subjects received dexamethasone in the immediate postoperative period. For safety purposes, routine noncontrast head CT and MRI were performed within 24 to 48 hours of surgery.

Cranial imaging techniques

All MRI/MRS were performed on a GE 3T MR scanner (General Electric Healthcare) with an eight-channel phase array head coil and included volumetric T1 images [inversion

recovery prepared fast spoiled gradient-recalled echo (IRSPGR), TR = 11.58 ms, TE = 4.8 ms, inversion time (TI) = 450 ms, partition size = 0.895 mm, in-plane resolution = 0.41 mm], T2 images [volumetric fast spin-echo (FSE), TR = 4.0 s, TE = 104 ms, contiguous 1.5-mm sections, in-plane resolution = 0.94 mm]. High-angular resolution diffusion MRI (HARDI) data were acquired for DTI analyses (b = 2000 s/mm^2, 55 directions, TR/TE = 15,000/74 ms, 2-mm isotropic voxels). All cranial scans were done at the study site. Proton MRS was performed within 4 × 2 × 2–cm voxels located in the bilateral centrum semiovale. Both short echo (TR = 1500 ms, TE = 26 ms) and long echo (TR = 1500 ms, TE = 288 ms) were acquired.

Image analyses

HARDI data were processed with a weighted least-squares fit to compute the diffusion tensor metrics. ROIs were drawn on the preimplant data that correspond to anterior corona radiata and posterior corona radiata and control regions in the larger surrounding left and right anterior frontal white matter (FL and FR) and left and right posterior parieto-occipital white matter (PL and PR) regions, the genu and splenium of the corpus callosum (CC), and bilateral cingulum (CI). The corpus callosum and cingulum regions were defined on the basis of probabilistic fiber tracking with QBall residual bootstrap (34). Fiber tracking from the injection sites largely delineated the inferior-superior pathways including corona radiata bundles.

For the longitudinal comparison, all time points for each subject were registered with a nonparametric, diffeomorphic deformable image registration (DTI-TK) (35). DTI registration is a challenge due to the fact that DTI data are multidimensional and the tensor orientation after image registration has to be consistent with the anatomy. The application of the DTI registration on these patients is more difficult because of the age of the patients and the severe hypomyelination in the CNS. The ROIs were registered to all time points with these transformations, and the accuracy of the registrations was visually verified by two neuroradiologists.

All ROIs were made with similar size and shape and were defined within coherent fiber bundles as determined by the fractional anisotropy value on the preimplant fractional anisotropy map. This step enables interpretation of the DTI metrics in the context of an aligned bundle of axons. Care was taken to define the ROIs within the boundary of the high-anisotropy regions to minimize partial volume contamination from neighboring tissue. Anatomically similar regions were chosen for all subjects. The ROIs defined at the preimplant time point were transformed to all other time points with the previously determined mapping and resampled with nearest-neighbor interpolation. A threshold reflecting the minimum fractional anisotropy value observed at the pre-implant ROI was used to further cull the registered postimplant ROIs. To assure that the same region was interrogated at preimplant and the subsequent time point, we then transformed back the thresholded postimplant ROIs to preimplant time point and resampled them with nearest-neighbor interpolation. This procedure ensured minimization of partial volume effects because of the variable acquisition angulations coupled with the registration process as well as consistency in the ROIs between postimplant and preimplant time points.

The DTI metrics at each time point were divided by the relevant preimplant values to provide a percentage of the preimplant value. The percentages were averaged across individual ROIs within an individual to create a mean percentage for implanted and control regions at each time point for each subject. Standard errors (SEs) were computed for implant and control region percentage values. To quantitatively assess the relative change of implant and control regions, we divided the implant percentage values by individual ROI control percentage values, and then, we averaged the ratios at each time point; the SE over these

ratios was computed. These ratios therefore eliminate any global effects on the percentage values in implant and control regions and present a normalized or relative percentage of change between implant and control regions over time. Mean values of the DTI metrics were extracted in all regions at each time point in each subject in the native space of the acquisition. The percentage of changes relative to preimplant DTI values in the corona radiata and control regions are shown for all subjects (Fig. 5); also on the plot are the mean of the control values and the ratio of corona radiata to control mean values.

Standard volumetry techniques are difficult on the PMD subjects because of the atypical distribution of signal intensities reflecting the lack of myelin contrast. To enable reliable estimates of the tissue volumes, we used multiparametric acquisitions with eight flip angles and an IRSPGR for B1 corrections to estimate three-dimensional T1 relaxation times maps (36). The T1 relaxation time maps were used to segment gray matter, white matter, and CSF via SienaX (http://www.fmrib.ox.ac.uk/fsl/siena/index.html).

Supplementary Material

Refer to Web version on PubMed Central for supplementary material.

Acknowledgments

We thank D. Ferriero and S. Hauser for suggestions on the manuscript.

Funding: This study was sponsored by StemCells Inc. (Newark, CA). R.J.J. is supported by NIH/National Center for Research Resources UCSF-CTSI (Clinical & Translational Science Institute) grant UL1 RR024131. D.H.R. is a Howard Hughes Medical Institute investigator. R.J.J. is the developmental psychologist in the Pediatric Clinical Research Center of the CTSI.

REFERENCES AND NOTES

1. Gencic S, Abuelo D, Ambler M, Hudson LD. Pelizaeus-Merzbacher disease: An X-linked neurologic disorder of myelin metabolism with a novel mutation in the gene encoding proteolipid protein. Am J Hum Genet. 1989; 45:435–442. [PubMed: 2773936]
2. Schiffmann R, van der Knaap MS. Invited article: An MRI-based approach to the diagnosis of white matter disorders. Neurology. 2009; 72:750–759. [PubMed: 19237705]
3. Garbern JY. Pelizaeus-Merzbacher disease: Genetic and cellular pathogenesis. Cell Mol Life Sci. 2007; 64:50–65. [PubMed: 17115121]
4. Schneider A, Montague P, Griffiths I, Fanarraga M, Kennedy P, Brophy P, Nave KA. Uncoupling of hypomyelination and glial cell death by a mutation in the proteolipid protein gene. Nature. 1992; 358:758–761. [PubMed: 1380672]
5. Dhaunchak AS, Colman DR, Nave KA. Misalignment of PLP/DM20 transmembrane domains determines protein misfolding in Pelizaeus–Merzbacher disease. J Neurosci. 2011; 31:14961–14971. [PubMed: 22016529]
6. Lin W, Popko B. Endoplasmic reticulum stress in disorders of myelinating cells. Nat Neurosci. 2009; 12:379–385. [PubMed: 19287390]
7. Duncan ID, Goldman S, Macklin WB, Rao M, Weiner LP, Reingold SC. Stem cell therapy in multiple sclerosis: Promise and controversy. Mult Scler. 2008; 14:541–546. [PubMed: 18562508]
8. Duncan ID, Hammang JP, Jackson KF, Wood PM, Bunge RP, Langford L. Transplantation of oligodendrocytes and Schwann cells into the spinal cord of the myelin-deficient rat. J Neurocytol. 1988; 17:351–360. [PubMed: 3171610]
9. Windrem MS, Schanz SJ, Guo M, Tian GF, Washco V, Stanwood N, Rasband M, Roy NS, Nedergaard M, Havton LA, Wang S, Goldman SA. Neonatal chimerizationwith human glial progenitor cells can both remyelinate and rescue the otherwise lethally hypomyelinated shiverer mouse. Cell Stem Cell. 2008; 2:553–565. [PubMed: 18522848]

10. Rowitch DH. Glial specification in the vertebrate neural tube. Nat Rev Neurosci. 2004; 5:409–419. [PubMed: 15100723]
11. Cummings BJ, Uchida N, Tamaki SJ, Salazar DL, Hooshmand M, Summers R, Gage FH, Anderson AJ. Human neural stem cells differentiate and promote locomotor recovery in spinal cord-injured mice. Proc Natl Acad Sci USA. 2005; 102:14069–14074. [PubMed: 16172374]
12. Uchida N, Chen K, Dohse M, Hansen KD, Dean J, Buser JR, Riddle A, Beardsley DJ, Wan Y, Gong X, Nguyen T, Cummings BJ, Anderson AJ, Tamaki SJ, Tsukamoto A, Weissman IL, Matsumoto SG, Sherman LS, Kroenke CD, Back SA. Human neural stem cells induce functional myelination in mice with severe dysmyelination. Sci Transl Med. 2012; 4:155ra136.
13. Nair G, Tanahashi Y, Low HP, Billings-Gagliardi S, Schwartz WJ, Duong TQ. Myelination and long diffusion times alter diffusion-tensor-imaging contrast in myelin-deficient *shiverer* mice. Neuroimage. 2005; 28:165–174. [PubMed: 16023870]
14. Harsan LA, Poulet P, Guignard B, Steibel J, Parizel N, de Sousa PL, Boehm N, Grucker D, Ghandour MS. Brain dysmyelination and recovery assessment by noninvasive in vivo diffusion tensor magnetic resonance imaging. J Neurosci Res. 2006; 83:392–402. [PubMed: 16397901]
15. Harsan LA, Steibel J, Zaremba A, Agin A, Sapin R, Poulet P, Guignard B, Parizel N, Grucker D, Boehm N, Miller RH, Ghandour MS. Recovery from chronic demyelination by thyroid hormone therapy: Myelinogenesis induction and assessment by diffusion tensor magnetic resonance imaging. J Neurosci. 2008; 28:14189–14201. [PubMed: 19109501]
16. Uchida N, Buck DW, He D, Reitsma MJ, Masek M, Phan TV, Tsukamoto AS, Gage FH, Weissman IL. Direct isolation of human central nervous system stem cells. Proc Natl Acad Sci USA. 2000; 97:14720–14725. [PubMed: 11121071]
17. Carpenter MK, Cui X, Hu ZY, Jackson J, Sherman S, Seiger A, Wahlberg LU. In vitro expansion of a multipotent population of human neural progenitor cells. Exp Neurol. 1999; 158:265–278. [PubMed: 10415135]
18. Tamaki S, Eckert K, He D, Sutton R, Doshe M, Jain G, Tushinski R, Reitsma M, Harris B, Tsukamoto A, Gage F, Weissman I, Uchida N. Engraftment of sorted/expanded human central nervous system stem cells from fetal brain. J Neurosci Res. 2002; 69:976–986. [PubMed: 12205691]
19. Song SK, Yoshino J, Le TQ, Lin SJ, Sun SW, Cross AH, Armstrong RC. Demyelination increases radial diffusivity in corpus callosum of mouse brain. Neuroimage. 2005; 26:132–140. [PubMed: 15862213]
20. Fancy SP, Chan JR, Baranzini SE, Franklin RJ, Rowitch DH. Myelin regeneration: A recapitulation of development? Annu Rev Neurosci. 2011; 34:21–43. [PubMed: 21692657]
21. Steiner, R.; Selden, N.; Huhn, SL.; Koch, T.; Al-Urzi, A.; Sikora, D.; Dean, S.; Penfield, J.; Sutcliffe, T.; Bammer, R.; Vogel, H.; Uchida, N. paper presented at the 12th International Congress on Neuronal Ceroid Lipofuscinosis; Hamburg, Germany. 2009.
22. Trepanier, AM.; Bennett, L.; Garbern, JY. paper presented at the American College of Medical Genetics; Albuquerque, NM. 2010.
23. Dubois J, Dehaene-Lambertz G, Perrin M, Mangin JF, Cointepas Y, Duchesnay E, Le Bihan D, Hertz-Pannier L. Asynchrony of the early maturation of white matter bundles in healthy infants: Quantitative landmarks revealed noninvasively by diffusion tensor imaging. Hum Brain Mapp. 2008; 29:14–27. [PubMed: 17318834]
24. McGraw P, Liang L, Provenzale JM. Evaluation of normal age-related changes in anisotropy during infancy and childhood as shown by diffusion tensor imaging. AJR Am J Roentgenol. 2002; 179:1515–1522. [PubMed: 12438047]
25. Mukherjee P, Miller JH, Shimony JS, Conturo TE, Lee BC, Almli CR, McKinstry RC. Normal brain maturation during childhood: Developmental trends characterized with diffusion-tensor MR imaging. Radiology. 2001; 221:349–358. [PubMed: 11687675]
26. Narayanan SP, Flores AI, Wang F, Macklin WB. Akt signals through the mammalian target of rapamycin pathway to regulate CNS myelination. J Neurosci. 2009; 29:6860–6870. [PubMed: 19474313]

27. Tyler WA, Gangoli N, Gokina P, Kim HA, Covey M, Levison SW, Wood TL. Activation of the mammalian target of rapamycin (mTOR) is essential for oligodendrocyte differentiation. J Neurosci. 2009; 29:6367–6378. [PubMed: 19439614]

28. Smith PM, Franklin RJ. The effect of immunosuppressive protocols on spontaneous CNS remyelination following toxin-induced demyelination. J Neuroimmunol. 2001; 119:261–268. [PubMed: 11585629]

29. Brüstle O, Jones KN, Learish RD, Karram K, Choudhary K, Wiestler OD, Duncan ID, McKay RD. Embryonic stem cell-derived glial precursors: A source of myelinating transplants. Science. 1999; 285:754–756. [PubMed: 10427001]

30. Bull ND, Irvine KA, Franklin RJ, Martin KR. Transplanted oligodendrocyte precursor cells reduce neurodegeneration in a model of glaucoma. Invest Ophthalmol Vis Sci. 2009; 50:4244–4253. [PubMed: 19357352]

31. Harsan LA, Poulet P, Guignard B, Parizel N, Skoff RP, Ghandour MS. Astrocytic hypertrophy in dysmyelination influences the diffusion anisotropy of white matter. J Neurosci Res. 2007; 85:935–944. [PubMed: 17278151]

32. Martino G, Pluchino S. The therapeutic potential of neural stem cells. Nat Rev Neurosci. 2006; 7:395–406. [PubMed: 16760919]

33. Zawadzka M, Rivers LE, Fancy SP, Zhao C, Tripathi R, Jamen F, Young K, Goncharevich A, Pohl H, Rizzi M, Rowitch DH, Kessaris N, Suter U, Richardson WD, Franklin RJ. CNS-resident glial progenitor/stem cells produce Schwann cells as well as oligodendrocytes during repair of CNS demyelination. Cell Stem Cell. 2010; 6:578–590. [PubMed: 20569695]

34. Berman JI, Chung S, Mukherjee P, Hess CP, Han ET, Henry RG. Probabilistic streamline *q*-ball tractography using the residual bootstrap. Neuroimage. 2008; 39:215–222. [PubMed: 17911030]

35. Zhang H, Avants BB, Yushkevich PA, Woo JH, Wang S, McCluskey LF, Elman LB, Melhem ER, Gee JC. High-dimensional spatial normalization of diffusion tensor images improves the detection of white matter differences: An example study using amyotrophic lateral sclerosis. IEEE Trans Med Imaging. 2007; 26:1585–1597. [PubMed: 18041273]

36. Deoni SC. High-resolution T1 mapping of the brain at 3T with driven equilibrium single pulse observation of T1 with high-speed incorporation of RF field inhomogeneities (DESPOT1-HIFI). J Magn Reson Imaging. 2007; 26:1106–1111. [PubMed: 17896356]

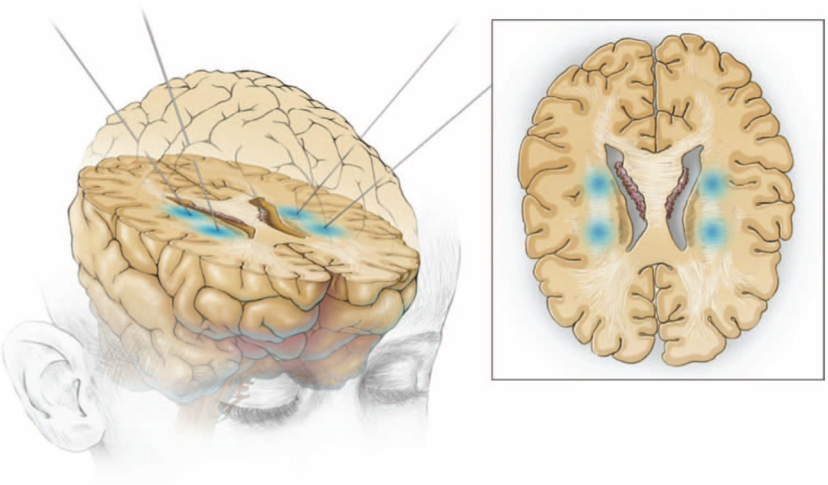

Fig. 1.
Sites of neural stem cell direct implantation. Under MRI guidance, HuCNS-SCs were transplanted into the deep white matter, the corona radiata, of the frontal white matter in two sites in each hemisphere of the brain of four PMD patients.

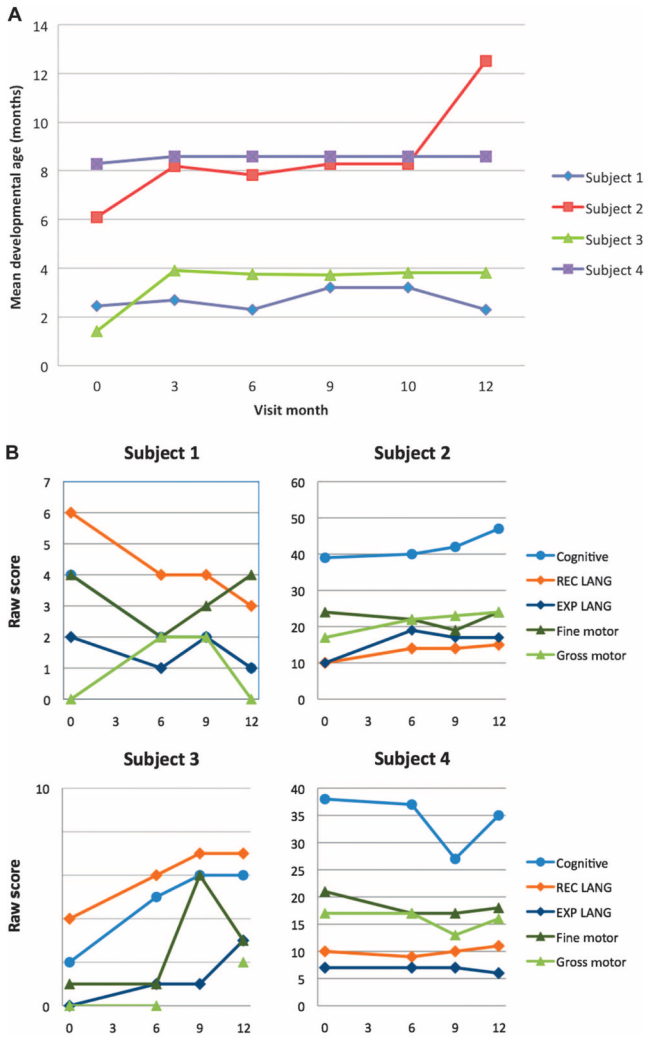

Fig. 2.

The CAS of child development and the Bayley-III. (**A**) Results for CAS showed overall stability of mean developmental age (in months) for all subjects, with the exception of subject 2, who demonstrated an overall gain from 6 to 12 months. (**B**) Bayley-III cognitive, language [receptive (REC) and expressive (EXP)], and motor (fine and gross) subtest raw scores at screening and 6, 9, and 12 months after transplant for all subjects. Small increases in select subtest scores were noted for subjects 2 and 4. Subjects 1 and 3 posttransplant scores, although variable, remained within the extreme lower end of the test range. Note difference in scale of the raw score axis used for each subject.

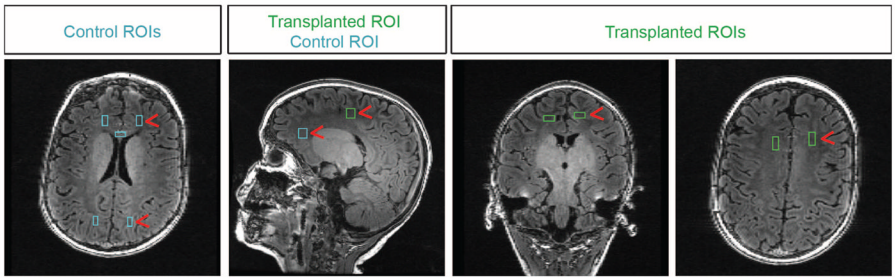

Fig. 3.

DTI measurements at control and implantation site ROIs in subject 2. T1-weighted MR images in orthogonal planes with boxes showing ROIs used for DTI analyses. ROIs adjacent to transplant sites are shown in green, and ROIs used to acquire control data are shown in aqua. Red arrowheads highlight the location of ROIs.

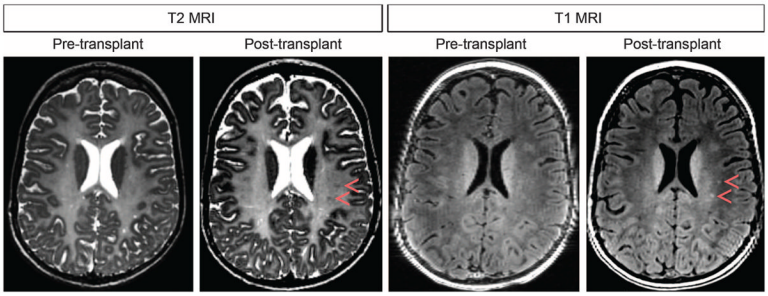

Fig. 4.

MRI images at baseline (pretransplant) and 12 months after transplant for subject 2. Small ovoid areas of T2 hypointensity and T1 hyperintensity (red arrowheads) were not present before transplantation and then gradually became visible after transplant. These areas do not represent small cysts because decreasing T2 hyperintensity is observed.

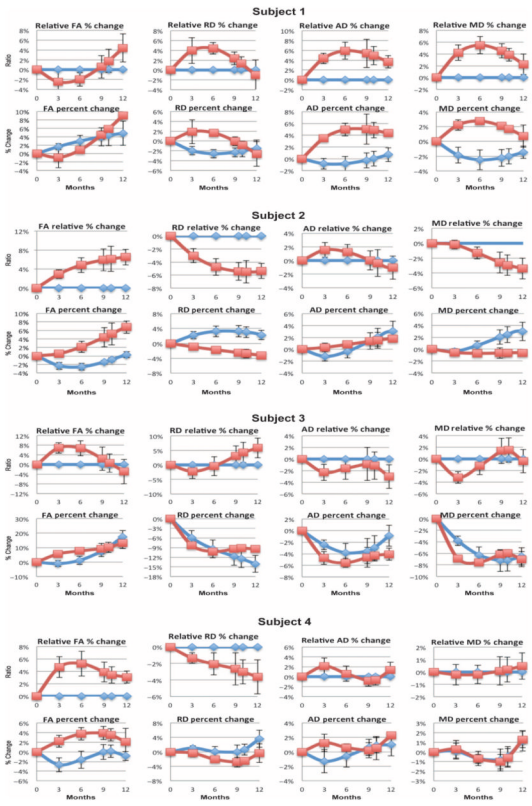

Fig. 5.

Absolute and relative diffusion metrics versus time. Zero is the starting point for each value on the preimplantation MRI study. Absolute values show percentage of change in each value at each imaging time point (red boxes for the implant site and blue diamonds for control sites). Relative values show control values as baseline (zero) and values at implant site as percentage of change from control. FA, fractional anisotropy; MD, mean diffusivity; RD, radial diffusivity; AD, axial diffusivity.

Table 1

Subject characteristics at study entry.

	Subject			
	1	**2**	**3**	**4**
PLP1 mutation	221G>A	730T>G	223A>C	728C>T
PLP1 protein	G74E (TM2)	P244V (TM4)	T75P (TM2)	A243V (TM4)
Nystagmus diagnosis	Birth	3 months	2 months	2 months
Hypotonia	Y	Y	Y	Y
Developmental delay	Y	Y	Y	Y
Early history of stridor	Y	N	Y	Y
Tracheostomy	Y	N	Y	N
G tube–dependent	Y	N	Y	N
Alertness	Y	Y	Y	Y
Spasticity	Y	N	Y	Y
Dysmetria	N/E*	Y	N/E*	Y
Language—receptive	N/E*	One-step commands	N/E*	One-step commands
Language—expressive	None	Sounds	None	Single words
Ambulation	N	N	N	With support
CPAP (night)	Y	N	Y	N
Self-feeding	N	N	N	N
EEG	Abnormal	Abnormal	Normal	Abnormal
Age at transplant (months)	16	42	14	66

*Could not evaluate.